Top Resonance Searches using the ATLAS Detector

Author:
Karl NORDSTRÖM

Supervisors:
Dr. Klaus MÖNIG
Dr. Thorsten KUHL
Christoph WASICKI
Madalina STANESCU

Abstract

This report presents work performed during the DESY summer student programme in Zeuthen, 2013. A brief introduction to the theoretical motivations for searching for a new particle decaying to top-antitop ($t\bar{t}$) pairs is given, and the LHC and ATLAS Experiment are introduced. The event selections currently used in the ATLAS top resonance analysis are detailed, and a short study of the effect of changing the triangular $M_{T,W}$ and E_T^{miss} cut in the muon channel to the tighter cuts used in the electron channel is presented, using a 1.5 TeV $\mathbf{Z'}$ as a benchmark signal. It is shown that the tighter cut removes 50% more QCD background than the triangular cut but also removes 20% of signal events. A short summary of the motivations for using multivariate mathematical techniques such as neural networks in an analysis searching for new physics is given together with an introduction to neural networks, and a variable correlation study is briefly presented. It is shown that the NeuroBayes package successfully can separate signal and background in the top resonance analysis.

October 1, 2013

Contents

1 Introduction

With the announcement of the discovery of a Higgs Boson in July 2012 [6][12] we might soon have experimental evidence for all of the particles in the Standard Model (SM). Experimental evidence for dark matter [10] and aesthetic problems in high energy theory [15] (among other observations) have however long hinted at the existence of physics Beyond the Standard Model (BSM). Many such theories have been proposed, usually predicting some kind of new physics at the TeV scale. Of particular importance for the searches considered in this report are models predicting the existence of a new massive neutral gauge boson, denoted $\mathbf{Z'}$ [18], and models with warped extra dimensions predicting new gluon excitations, denoted $\mathbf{g_{KK}}$ [1] [19]. Both of these types of particles would decay predominantly to top quarks due to their high mass (as necessary to have avoided observation so far), and as such could be observed as peaks in the differential cross section (resonances) of $t\bar{t}$ that could not occur within the SM.

2 ATLAS Experiment

2.1 The LHC

The Large Hadron Collider (LHC) is the most powerful particle collider in the world with a center-of-mass energy of $\sqrt{s} = 8$ TeV, scheduled to be increased up to 14 TeV. Its average luminosity during the 2012 run

[1] KK stands for Kaluza and Klein, who proposed extra dimensions as a way to unify gravitation with electromagnetism. Note that the same strategy was first used by Gunnar Nordström who realised he could unify the two forces within the framework of his own theory of gravitation seven years before Kaluza published his results.

was about 60 $\times 10^{32}$cm^{-2}s^{-1}. Unlike the Large Electron Positron (LEP) collider, which originally inhabited its tunnel 100 meters below Switzerland and France, it collides hadrons instead of leptons. The higher mass of the protons it uses compared to the electrons and positrons of the LEP allows for higher energies with a smaller fraction lost to brehmsstrahlung, but their composite nature means that all predictions have to rely on knowledge of the proton's structure functions. This introduces unavoidable experimental uncertainty, which is the main motivation for building the International Linear Collider (ILC) which could provide precision measurements of particles or other phenomena discovered by the LHC. Since the LHC started operation in 2008 it has found a new particle consistent with the SM Higgs boson [6], confirmed the SM works at unprecedented energy scales [23], and generally caused headaches for theorists worldwide.

The data set used in this report was taken during the $\sqrt{s} = 8$ TeV run of 2012, with all triggers operating nominally. The total integrated luminosity is about 20.3 fb^{-1}.

2.2 ATLAS Detector

The ATLAS detector is one of two general-purpose detectors at the LHC[2]. The part of the detector closest to the interaction point (IP) is called the inner detector, and consists of three parts: the silicon pixel detector, the semi-conductor strip tracker, and the transition radiation tracker. Together they allow the experiment to track individual particles close to the interaction point with very high precision, and to measure their charge and momentum using strong magnetic fields. Tracks with $\eta < 2.5$, $p_T > 500$ MeV have a p_T resolution of less than 3% [5]. For definitions of these terms please see section 2.3.

Outside of the tracking detectors are the calorimeters, consisting of the inner electromagnetic calorimeter and outer hadronic calorimeter. These measure the energy of the particles by absorbing them, and can also aid in identifying particles by analysis of the shape of the energy deposits. The electromagnetic calorimeter is very precise and absorbs particles that couple to the electromagnetic force: charged particles and photons. The hadronic calorimeter is less precise and measures particles that don't couple to the electromagnetic force but do couple to the strong force, mainly hadrons. Highly collimated showers of particles resulting from a quark or gluon (jets)[3] are usually measured mainly with the calorimeters. The calorimeters have an energy resolution on the order of 10%.

The outermost layer of the detector is the muon spectrometer, which measures the momentum of muons to high precision. Since muons rarely interact with matter but it is important to be able to identify them, this part of the detector is by far the largest. Like the tracking detectors it uses magnetic fields to bend the path travelled by the muons.

Due to the high luminosity of the LHC there are usually several interactions occuring at every bunch crossing: in 2012 the average number was 20.7, and this is set to rise as the LHC is pushed to higher energies. It is often impossible to completely separate this background noise, referred to as *pile-up*, from the interesting interaction being studied due to finite detector resolution. Reducing the impact of ever-increasing amounts of pile-up on physics analyses is therefore an active area of research.

2.3 Coordinate System

The ATLAS coordinate system defines z in the direction of the beamline, x towards the center of the circle which the protons travel around, and y vertically upwards. The $x - y$ plane is usually called the *transverse* plane and most quantities are measured in this plane, since we can't rely on energy and momentum conservation along the beamline. The angle in the transverse plane is denoted ϕ, whereas the angle to the beamline is denoted θ. Since the difference in θ between two particles is not constant under Lorentz boosts, it is common to use rapidity (y) instead, defined as:

$$y = \frac{1}{2} \ln \left(\frac{E + p_z}{E - p_z} \right)$$

[2]And definitely the better one!

[3]The process by which jets are formed is related to the *confinement* of QCD, effectively disallowing coloured states from existing freely. See for example [25] for a review or [2] for a more in-depth discussion.

From an experimental point of view it is often easier to use a zero-mass approximation called pseudorapidity (η) instead, defined as[4]:

$$\eta = \frac{1}{2} \ln \left(\frac{|p| + p_z}{|p| - p_z} \right)$$

These definitions are taken from [13]. We can then define a Euclidean distance measure in the $\eta - \phi$[5] plane as:

$$dR = \sqrt{d\eta^2 + d\phi^2}$$

Quantities with a T subscript are, unless otherwise stated, taken in the transverse plane, so for example $p_T = \sqrt{p_x^2 + p_y^2}$.

3 $t\bar{t}$ Production

The SM predicts that $t\bar{t}$ pairs are mainly produced through gluon fusion and quark-antiquark annihilation at the energies the LHC operates at. Figure 3.1 presents the Feynman diagrams for these interactions.

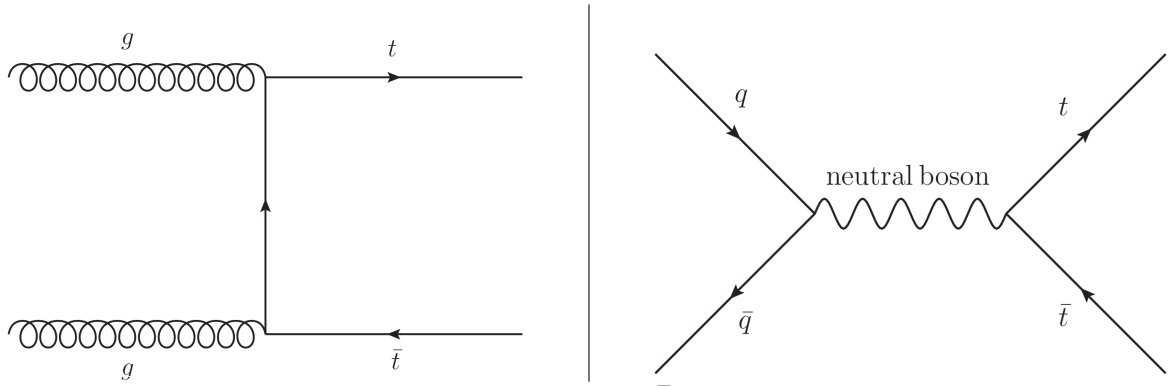

Figure 3.1: The main SM production channels for $t\bar{t}$ at the LHC. On the left is gluon fusion, which accounts for about 80% (90%) of $t\bar{t}$ production at $\sqrt{s} = 8$ (14) TeV, and on the right quark annihilation, which accounts for the majority of the remainder.

Since the top quark is the heaviest particle in the SM there are no special features in the differential cross section, which roughly speaking is exponentially falling as a function of the invariant mass of the $t\bar{t}$ system (M_{tt}). Within the SM the neutral boson referred to in figure 3.1 is $> 99.9\%$ of the time a gluon.

3.1 Z′

The Feynman diagram on the right in figure 3.1 refers to a generic neutral boson as the intermediate particle between quark annihilation and the production of a $t\bar{t}$ pair. Since the $\mathbf{Z}'$ can be roughly thought of as a heavier partner of the SM $\mathbf{Z}$ boson it fits the bill and would modify the probability of this interaction occuring at energies high enough to allow its creation. This is a possible source of sharp top resonances, with the relative width[6] typically on the order of a few percent. The couplings to SM fermions of this hypothetical $\mathbf{Z}'$ depend on the particular theory under consideration: one popular benchmark choice is the Sequential SM, which assumes the couplings are identical to those of the SM $\mathbf{Z}$ boson [18], whereas another is to assume the $\mathbf{Z}'$ is leptophobic (couples weakly to leptons), which would make the $t\bar{t}$ channel even more important as a possible way to detect it. The relative width is usually taken as constant so that the absolute width grows with the mass.

[4]It can also be expressed as $\eta = -\ln[\tan(\theta/2)]$ which shows clearly that it is a function only of θ, hence why it is practical for experiments.

[5]This can (and often is) taken in the $y - \phi$ plane instead. Using y is generally a good idea when dealing with massive particles since the zero-mass approximation of η breaks down and it no longer is immune to Lorentz boosts.

[6]Defined as $\frac{\Gamma}{M_{\mathbf{Z}'}} = \frac{1}{\tau_{\mathbf{Z}'} M_{\mathbf{Z}'}}$ where τ is the particle lifetime.

3.2 $\mathbf{g_{KK}}$

Kaluza-Klein gluon excitations can also be produced through quark annihilation in a similar way as the $\mathbf{Z'}$ since gluons don't carry electric charge, or through a slightly modified gluon fusion process where two gluons form a single massive gluon excitation. The branching ratio for $\boldsymbol{g^1 \rightarrow t\bar{t}}$ is 92.5% [20] so $\boldsymbol{t\bar{t}}$ is by far the best channel to detect it in. Unlike the $\mathbf{Z'}$ signal, $\mathbf{g_{KK}}$ would result in a very broad resonance since it decays through the strong force. Typical models have a relative width of about 15%. It is usual to use Randall-Sundrum models as benchmarks for $\mathbf{g_{KK}}$, as done in for example [20].

4 $\boldsymbol{t\bar{t}}$ Decay Channels

Top quarks are due to their high mass very short-lived, with an average lifetime on the order of 10^{-25} seconds [7]. This means it is too shortlived to hadronise, and only decays through the weak force. Since top quarks almost always decay $t \rightarrow Wb$, this is the only channel that is considered at experiments. The W is itself a short-lived particle and quickly decays further. There are, in general, two types of W decay: $W \rightarrow l\nu_l$ (*leptonic*) and $W \rightarrow q\bar{q}$ (*hadronic*). The probability of a hadronic decay is about 68%, and the probability of a leptonic decay is hence about 32%, with an equal 10.5% for each lepton generation. In a $\boldsymbol{t\bar{t}}$ decay you therefore get a 45% chance of both tops decaying hadronically, an equal 45% chance of one of the tops decaying hadronically and the other leptonically (a *semileptonic* decay), and a 10% chance of a double leptonic decay.

4.1 Resolved and boosted

The standard way of identifying top quarks is to first identify the resolved decay products of the b and W and then reconstruct the top using them. This is called the *resolved* channel. Searches for $\boldsymbol{t\bar{t}}$ resonances were long thought to be problematic since the two tops would usually be produced with a very high boost factor due to the mass of the resonating particle, making the decay products highly collimated. This is called the *boosted* channel. We have only recently developed mathematical tools that allow us to make educated attempts at identifying boosted fat jets originating from top quarks, jet substructure being perhaps the most important one [26]. The idea is to probe the internal structure of the jet using various observables to determine its origin. For example the existence of harder subsections of the jet, or particular features of the clustering of the jet can be taken advantage of. For a review of jet substructure methods please see for example [3].

5 Event Selections

Top resonance event selections are designed to maximise the signal-to-background ratio, to make it easier to detect an excess from the SM expectation in the data. Due to experimental reasons we only consider a subset of the decay channels outlined above. Events where both Ws decay hadronically have six jets (or two or more fat jets) in their final state, and are hence difficult to separate from QCD background reliably, while also requiring an advanced approach to cuts on jet multiplicity, whereas events where both Ws decay leptonically have two hard neutrinos in the final state. Since we only can reconstruct the total missing E_T[7] (E_T^{miss}) we lose all information about the direction and energy of the individual neutrinos. Both of these types of decays are therefore excluded from the analysis, and we are left with semileptonic events where we have 4 jets of which at least two are b-jets (or 1 fat jet and a single narrow b-jet with $\Delta\phi(\text{fj}, \text{nj}) \approx \pi$), a single hard lepton, and a large E_T^{miss}. This situation is illustrated as a diagram in figure 5.2. Tau leptons have a very short lifetime and are difficult to separate from background in case of hadronisation so are only considered if they happen to decay into another lepton, in which case they by necessity are considered e or μ decays anyway.

[7] Calculated using the assumption of energy and momentum conservation in the transverse plane.

In the end we then have four decay channels: semileptonic $t\bar{t}$ with either an electron or muon, both divided into resolved and boosted cases. This corresponds to about 36% of all $t\bar{t}$ decays: 15% each from electron and muon semileptonic decays, and $\approx 0.4 \times 15\%$[8] from tau semileptonic decays where the tau decays into an electron or muon. Jets are found using the anti-k_t algorithm [8] with R=0.4 for narrow jets ($j^{0.4}$) and R=1.0 for fat jets ($j^{1.0}$), and are then pile-up corrected by applying a jet area reweighting [9] on the narrow jets and trimming [17] the fat jets. Narrow jets are selected with $p_T > 25$ GeV and fat jets with $p_T > 300$ GeV. A simplified cut flow for all four channels is presented in table 1. The transverse mass of the W candidate ($M_{T,W}$) is defined as $M_{T,W} = \sqrt{2p_T^l E_T^{miss}(1 - \cos\Delta\phi)}$. The k_t splitting scale $\sqrt{d_{n,n+1}}$ is found by reclustering the jet with the standard k_t algorithm and obtaining the scale of the combination from n+1 to n jets. For a fat top jet we expect $\sqrt{d_{12}} \approx M_{\text{top}}/2 = 85$ GeV, with additional information in $\sqrt{d_{23}}$ about the W.

Cut	Resolved electron	Boosted electron	Resolved muon	Boosted muon
Trigger	Top electron	Top electron	Top muon	Top muon
Lepton	Exactly 1 e, 0 μ with $p_T > 25$ GeV & match to trigger	Exactly 1 e, 0 μ with $p_T > 25$ GeV & match to trigger	Exactly 1 μ, 0 e with $p_T > 25$ GeV & match to trigger	Exactly 1 μ, 0 e with $p_T > 25$ GeV & match to trigger
$\boldsymbol{E_T^{\text{miss}}}$	$E_T^{\text{miss}} > 30$ GeV	$E_T^{\text{miss}} > 30$ GeV	$E_T^{\text{miss}} > 20$ GeV	$E_T^{\text{miss}} > 20$ GeV
$\boldsymbol{M_{T,W}}$	$M_{T,W} > 30$ GeV	$M_{T,W} > 30$ GeV	$M_{T,W}$+$E_T^{\text{miss}} > 60$ GeV	$M_{T,W}$+$E_T^{\text{miss}} > 60$ GeV
Jets	$\geq 4\ j^{0.4}$ or $\geq 3\ j^{0.4}$ with one $M_{j^{0.4}} > 60$ GeV	$\geq 1\ j^{1.0}$ and $\geq 1\ j^{0.4}$ with $dR(e) < 1.5$	$\geq 4\ j^{0.4}$ or $\geq 3\ j^{0.4}$ with one $M_{j^{0.4}} > 60$ GeV	$\geq 1\ j^{1.0}$ and $\geq 1\ j^{0.4}$ with $dR(\mu) < 1.5$
b-tags	≥ 1 b-tagged $j^{0.4}$	≥ 1 b-tagged $j^{0.4}$	≥ 1 b-tagged $j^{0.4}$	≥ 1 b-tagged $j^{0.4}$
Fat Jet	-	$M_{j^{1.0}} > 100$ GeV $\sqrt{d_{12}}_{j^{1.0}} > 40$ GeV	-	$M_{j^{1.0}} > 100$ GeV $\sqrt{d_{12}}_{j^{1.0}} > 40$ GeV
Topology	-	$dR(j^{1.0},j^{0.4}) > 1.5$ $d\phi(j^{1.0}, e) > 2.3$	-	$dR(j^{1.0},j^{0.4}) > 1.5$ $d\phi(j^{1.0}, \mu) > 2.3$

Table 1: Table presenting the cut flow for all four channels used in the analysis. Details have been left out to present only the selections that are most relevant to understanding the physics of the analysis without requiring knowledge of detector design and efficiencies.

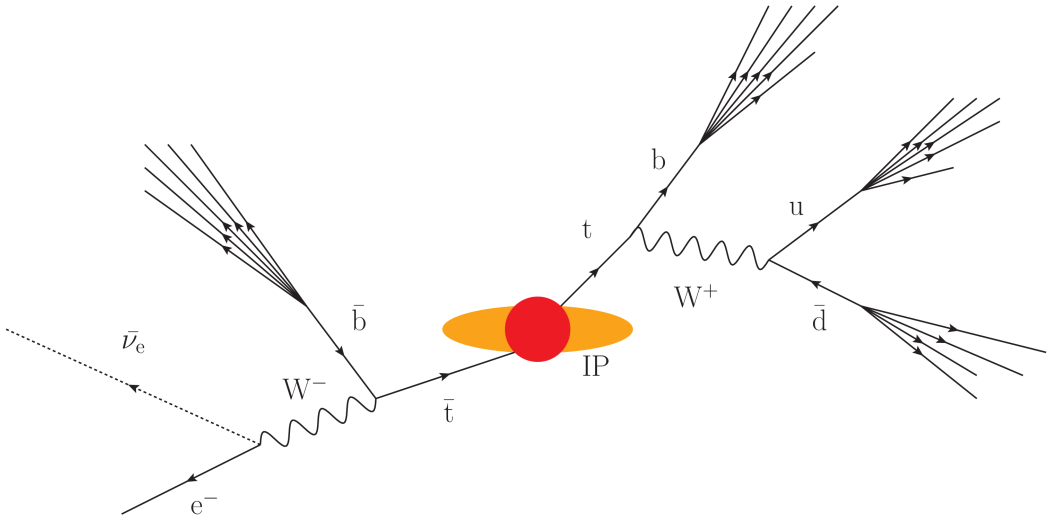

Figure 5.2: Example illustrated diagram of a full semileptonic $t\bar{t}$ decay, including hadronisation of the free quarks. The reconstructed E_T^{miss} quantity corresponds to the p_T of ν_e, whereas the reconstructed $M_{T,W}$ quantity corresponds to the transverse mass of the W^- boson.

[8]The 0.4 factor can be derived from the CKM matrix: $V_{ud}^2 + V_{us}^2 \approx 1$ which is multiplied by three to take different colours into consideration, so the chance of a tau decaying into an electron or muon is $\approx \frac{1}{1+1+3}$, giving a total chance of a leptonic decay of $\approx \frac{2}{5}$.

6 Monte Carlo Samples

The generator and showering packages used vary from sample to sample according to recommendations from the ATLAS MC group. For event generation we use ALPGEN [21], POWHEG [22], AcerMC [16], MadGraph [4], and the Pythia [24] and Herwig [11] families. For showering, where needed, the Pythia and Herwig families are used. LHAPDF [27] is used to access parton density functions. The samples have been run through a full ATLAS detector simulation based on GEANT4 [1].

Unless otherwise stated the *signal* refers to a 1.5 TeV $\mathbf{Z}'$. The background is made up of SM $\boldsymbol{t\bar{t}}$, W + jets, QCD background, single $\boldsymbol{t}$, Z + jets, and diboson events. The QCD background is derived from data using the matrix method for QCD background estimation.

7 Studying the Muon $M_{T,W}$ and E_T^{miss} Cut

As can be seen in table 1 the $M_{T,W}$ and E_T^{miss} cut is laxer in the muon channel compared to the electron channel: a triangular cut of $M_{T,W}$+$E_T^{\text{miss}} > 60$ GeV and $E_T^{\text{miss}} > 20$ GeV is used instead of requiring both to be greater than 30 GeV like in the electron channel.[9] Changing to the stricter cut could reduce QCD background in particular, since the combined E_T^{miss} and $M_{T,W}$ is a very specific feature of a leptonic W decay.

The figures 7.3, 7.4, and 7.5 show some resulting distributions using the two different cuts. The old cut refers to the triangular cut, whereas the new cut to the electron cut. In general the total number of events passing all selections is reduced by about 20% in both signal and background, but QCD background is reduced by as much as 50%. Since QCD is quite a small part of the total, stacked background this effect is not immediately noticeable in the stacked histograms however. Note that the new cut is only used in the resolved channel since QCD background is removed completely already with the laxer cut. The percentage of events passing each individual cut for QCD background and signal is presented in table 2.

Cut	**QCD$^{\text{old}}$ Rel %**	**Abs %**	**QCD$^{\text{new}}$ Rel %**	**Abs %**	**Z$'^{\text{old}}$ Rel %**	**Abs %**	**Z$'^{\text{new}}$ Rel %**	**Abs %**
Trigger +lepton	27.02	27.02	27.02	27.02	12.49	12.49	12.49	12.49
$\boldsymbol{E_T^{\text{miss}}}$	79.55	21.5	56	16.21	96.7	12.07	92.18	11.51
$\boldsymbol{M_{T,W}}$	92.28	19.84	94.79	15.37	96.4	11.63	74.73	8.6
Jets	0.66	0.13	0.54	0.06	80.24	9.33	80	6.88
b-tags	53.2	**0.07**	53.3	**0.03**	87.33	**8.15**	89.7	**6.17**

Table 2: Table presenting the percentage of data left after the old and new cuts for QCD background and signal in the resolved muon channel. Results for the boosted channel are not presented since effectively no QCD events pass the fat jet p_T selection, so the new cuts are meaningless there. Note that the QCD sample is reduced to contain only events which pass the lepton trigger requirements in advance.

[9] Note the stricter cut results in a proper subset of the events selected by the laxer cut being chosen.

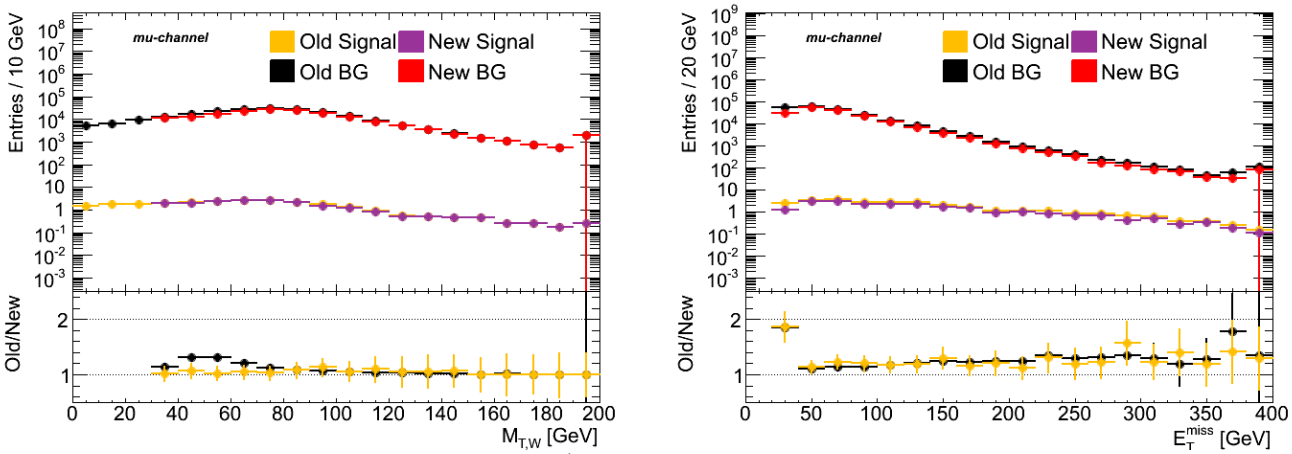

Figure 7.3: Plots for the $M_{T,W}$ and E_T^{miss} distributions for signal and stacked background with the old and new cuts. Note the logarithmic axis. The total number of events passing all cuts is in both cases reduced by about 20%.

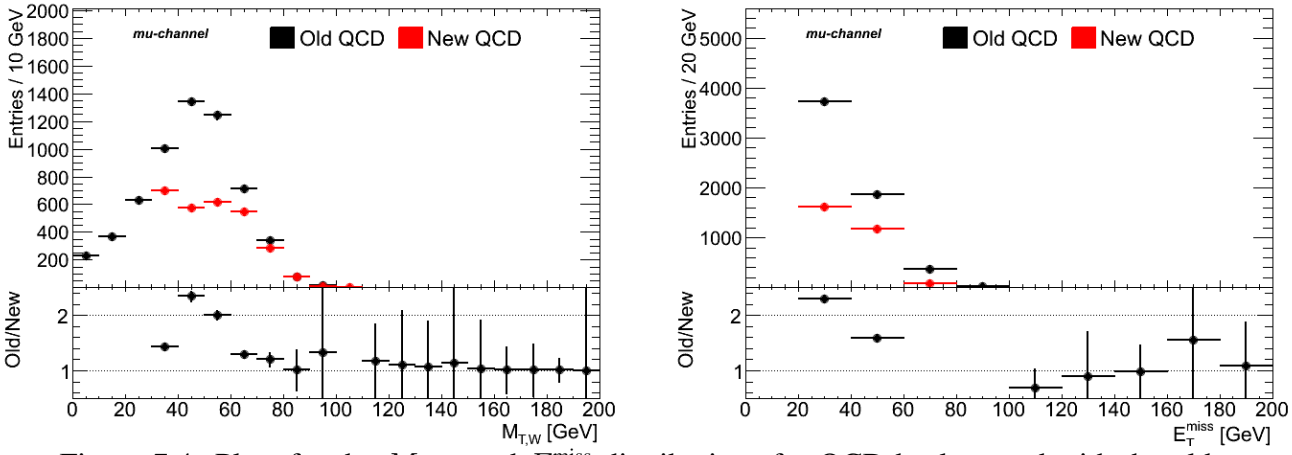

Figure 7.4: Plots for the $M_{T,W}$ and E_T^{miss} distributions for QCD background with the old and new cuts. Note that the total number of events passing all cuts is reduced by over 50%.

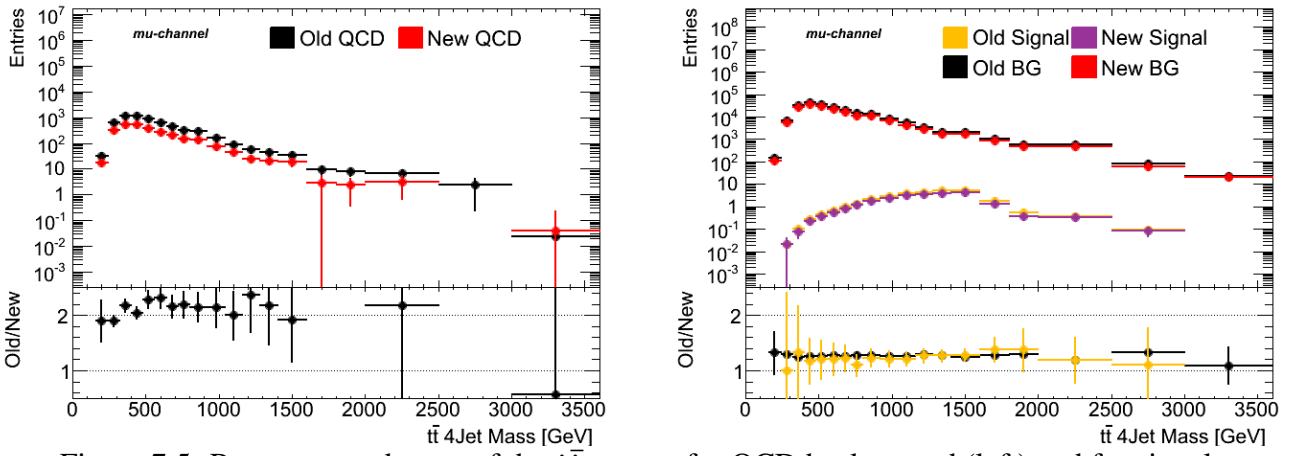

Figure 7.5: Reconstructed mass of the $t\bar{t}$ system for QCD background (left) and for signal and stacked background (right). Note the logarithmic axis. QCD background is suppressed much more than the other background and the signal as expected.

8 Correlation Studies for Neural Network

8.1 Neural Network Introduction

A neural network is a mathematical tool inspired by biological networks of neurons such as our brain. It takes a number of input variables, transformed into a form understood by the network[10] if need be, and then enters these values into a layer of input nodes where each variable has a corresponding node. Each node has its own threshold function, which determines its output. This output is then ran through a hidden layer of similar nodes and finally submitted to the output layer which outputs the result in the requested form, for example a boolean if we ask the question *is this a signal event?*, or a floating point number if the question is *what is the probability that this is a signal event?* All communication between nodes is governed by a set of weights, one for each connection vector. By changing the weights and the threshold functions of individual nodes we can *teach* the neural network to give the correct output. Teaching takes place by using a large data set of known results and running this through the neural network, using *backpropagation* to alter the weights and threshold functions of the network to optimise the result. Once the network has been sufficiently trained, it can be used to separate signal and background in cases where we don't know the result. A perfect neural network should do so as well as is possible given the training data, however there are many practical problems that need to be taken into consideration for this to be the case.

One problem is avoiding overtraining, which can occur when too many variables are fed into the network: the more input nodes are used, the higher the probability that some random noise is mistaken as a feature of the learned data. An effective way of dealing with overtraining is giving the network fewer variables. Arguably the best way to do this is to perform a correlation analysis between all variables and removing ones which are highly correlated to others. Since the neural network fundamentally uses correlations between variables to compute the weights and threshold functions, removing a variable which can be completely determined using other variables already in the network should have no effect on the learning rate and discriminating power of the network.

8.2 NeuroBayes and Variable Correlations

We use the NeuroBayes package [14] for preprocessing our data and then creating and teaching our neural network. Since it is commercial software we don't have access to the source code, so it is good practice to double check the output to make sure it does what it claims to do. One of the most useful features of NeuroBayes is its advanced preprocessing of variables, which can notice correlations and remove unnecessary variables before starting the teaching loop. To get a better understanding of how this feature works, and to allow us to do this manually which ultimately is safer for a physics analysis, we can create 2D histograms comparing various observables, and calculate a correlation factor to compare to the output of NeuroBayes. We use a standard linear correlation measure of two variables X and Y defined as:

$$\rho = \frac{cov(X,Y)}{\sigma_X \sigma_Y}$$

σ_X is here the standard deviation of X. Let $E[x]$ be the expectation value of X, then the covariance $cov(X,Y)$ is defined as:

$$cov(X,Y) = E[xy] - E[x]E[y]$$

From inspection we can notice that ρ should take values in the range $-1 \leq \rho \leq 1$, where -1 corresponds to a perfect negative linear correlation, 1 corresponds to a perfect linear correlation, and 0 corresponds to no linear correlation at all. Note that ρ does not understand higher order or inversely linear $\left(Y \propto \frac{1}{X}\right)$ correlations well. When plotting and calculating the correlations we divide the data into three groups: signal, SM $t\bar{t}$ background, and the rest of the background. We expect $t\bar{t}$ background to be similar to the signal but we should be able to quite easily distinguish these two from the rest of the background.

[10] Often a Gaussian or similarly 'simple' distribution.

Legend:

1. Neural Network Output
2. $\sqrt{d_{12}}$ of hadronic fat jet
3. p_T of leptonic narrow jet
4. τ_1 of hadronic fat jet
5. τ_{21} of hadronic fat jet
6. τ_{32} of hadronic fat jet
7. width of hadronic fat jet

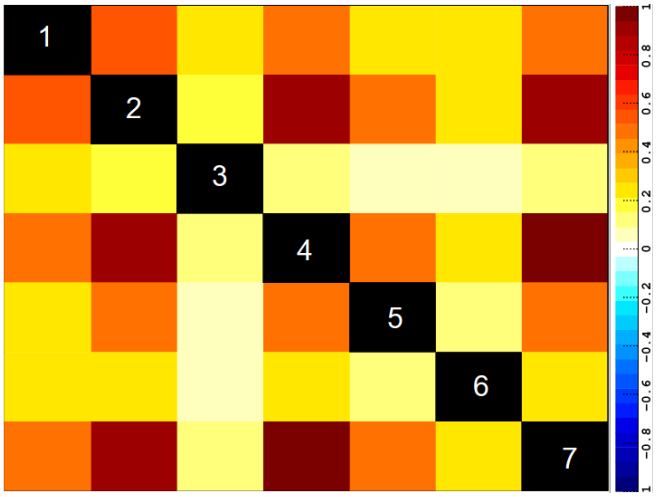

Figure 8.6: Example correlation matrix calculated by NeuroBayes. Note the high correlations for variables $2 \leftrightarrow 4$, $2 \leftrightarrow 7$, and $4 \leftrightarrow 7$, and that variable 3 correlates weakly to all the other variables (except the neural network output) as expected since it is the only leptonic side observable.

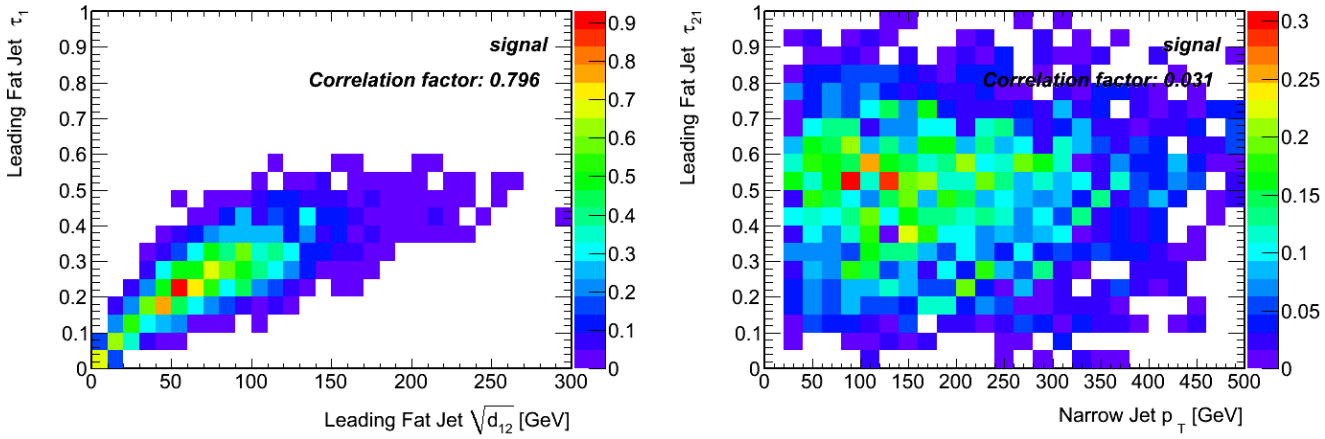

Figure 8.7: 2D plots for variables $2 \leftrightarrow 4$ and $3 \leftrightarrow 5$ from the previous figure. Notice the correlation factors agree well with the output of NeuroBayes.

Figure 8.6 shows the correlation factors as computed by NeuroBayes, and figure 8.7 shows two examples of the same correlation coefficients calculated manually. Similar plots and correlation coefficients have been calculated for all 47 variables currently useable by the neural network, but due to space restrictions I can't reproduce more here. The full set of plots has over 2200 members. It was found that NeuroBayes generally produced similar correlation factors as those calculated manually. The high correlations between several variables in the neural network defined by figure 8.6 suggests this network only can use a few effective variables to separate between signal and background. The network output in the case where background does not include SM $t\bar{t}$ is shown in figure 8.8: as can be seen the network manages to separate the two fairly well even with these suboptimal variables.

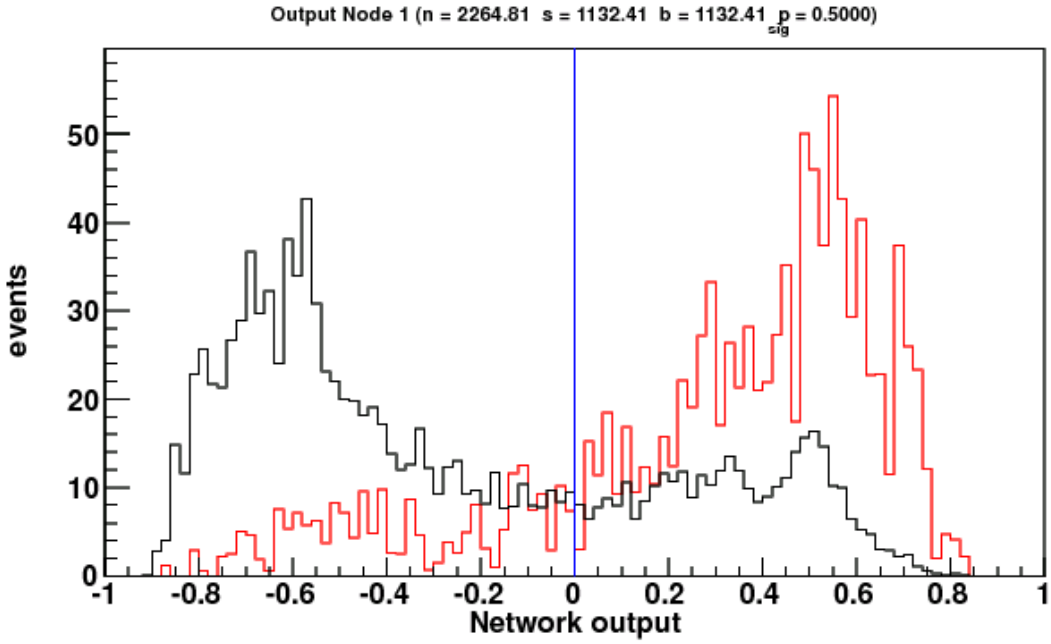

Figure 8.8: Neural network signal and background separation using the variables defined above. Red is signal, black is all background except SM $t\bar{t}$.

9 Conclusions

In this report the theoretical motivation for searches for $t\bar{t}$ resonances has been briefly laid out, and the general features of the LHC and ATLAS Experiment have been explained. The current approach to searches for $t\bar{t}$ resonances at ATLAS has been reviewed, with a focus on the physics over technical details. It has been shown that using identical $M_{T,W}$ and E_T^{miss} cuts in the muon channel as in the electron channel suppresses QCD background very efficiently in the resolved channel, but also results in a 20% loss of events in all samples. A brief motivation for using neural networks in the context of a particle physics analysis has been given, and a variable correlation study has been performed to validate and understand the NeuroBayes package, and to create a solid quantitative and qualitative understanding of variable correlations in the $t\bar{t}$ environment for future use in a neural network-based analysis.

10 Acknowledgments

I would like to thank my supervisors for invaluable help and support: Thorsten for giving me a much deeper appreciation of the subtleties of top analyses and experimental particle physics in general, Christoph for always being available and willing to help with whatever was bothering me at the moment (usually something programming related) and making me understand why some people actually use vi, Madalina for always providing me with literature, disk space, coffee, and discussion, and Klaus for choosing me and generally being a great guy. I also thank DESY Zeuthen for putting up with me for the past two months and paying me money to do something I would do for free, and Ingo Bloch, Thomas Naumann, and Elin Bergeås Kuutmann for taking me to lunch and interesting discussions over said lunch. I'd also like to thank Karl Jansen for taking good care of us and having a sense of humor. Thanks Karl!

Bibliography

[1] Agostinelli et al., 2003, *GEANT4 - a simulation toolkit*, Nucl. Instr. Meth. A, Volume 506, Issue 3, Pages 250 - 303

[2] Andersson et al., 1983, *Parton fragmentation and string dynamics*, Physics Reports, Volume 97, Issue 2 - 3, Pages 31 - 145

[3] Altheimer et al., 2012, *Jet substructure at the Tevatron and LHC: new results, new tools, new benchmarks*, Journal of Physics G: Nuclear and Particle Physics, Volume 39, Issue 6, Page 063001

[4] Alwall et al., 2011, *MadGraph 5 : Going Beyond*, arXiv:1106.0522 [hep-ph]

[5] ATLAS Collaboration, 2010, *Estimating Track Momentum Resolution in Minimum Bias Events using Simulation and K_S in $\sqrt{s} = 900$ GeV collision data*, ATLAS-CONF-2010-009

[6] ATLAS Collaboration, 2012, *Observation of a new particle in the search for the Standard Model Higgs boson with the ATLAS detector at the LHC*, Physics Letters B, Volume 716, Issue 1, Pages 1 - 29

[7] Beringer et al. (Particle Data Group), 2012, *The Review of Particle Physics*, Phys. Rev. D, Volume 86, Page 010001

[8] Cacciari et al., 2008, *The anti-k_t jet clustering algorithm*, Journal of High Energy Physics, Volume 2008, Issue 04, Page 63

[9] Cacciari et al., 2008, *Pileup subtraction using jet areas*, Physics Letters B, Volume 659, Issues 1 - 2, Pages 119 - 126

[10] Clove et al., 2006, *A direct empirical proof of the existence of dark matter*, arXiv:astro-ph/0608407

[11] Corcella et al., 2001, *HERWIG 6: an event generator for hadron emission reactions with interfering gluons (including supersymmetric processes)*, Journal of High Energy Physics, Volume 2001, Issue 1, Page 10

[12] CMS Collaboration, 2012, *Observation of a new boson at a mass of 125 GeV with the CMS experiment at the LHC*, Physics Letters B, Volume 716, Issue 1, Pages 30 - 61

[13] Ellis et al., 1996, *QCD and Collider Physics*, Cambridge University Press, Cambridge (UK), ISBN 0 521 58189 3

[14] Feindt, 2004, *A Neural Bayesian Estimator for Conditional Probability Densities*, arXiv:physics/0402093 [physics.data-an]

[15] Giudice, 2008, *Naturally Speaking: The Naturalness Criterion and Physics at the LHC*, arXiv:0801.2562 [hep-ph]

[16] Kersevan and Richter-Was, 2013, *The Monte Carlo event generator AcerMC versions 2.0 to 3.8 with interfaces to PYTHIA 6.4, HERWIG 6.5 and ARIADNE 4.1*, Computer Physics Communications, Volume 184, Issue 3, Pages 919 - 985

[17] Krohn et al., 2010, *Jet trimming*, Journal of High Energy Physics, Volume 2010, Issue 2, Pages 1 - 21

[18] Leike, 2008, *The Phenomenology of Extra Neutral Gauge Bosons*, Physics Reports, Volume 317, Issues 3 - 4, Pages 143 - 250

[19] Lillie et al., 2007, *Kaluza-Klein gluons as a diagnostic of warped models*, Phys. Rev. D, Volume 76, Issue 11, Page 115016

[20] Lillie et al., 2007, *The Bulk RS KK-gluon at the LHC*, Journal of High Energy Physics, Volume 2007, Issue 09, Page 74

[21] Mangano et al., 2003, *ALPGEN, a generator for hard multiparton processes in hadronic collisions*, Journal of High Energy Physics, Volume 2003, Issue 07, Page 1

[22] Oleari, 2010, *The POWHEG BOX*, Nuclear Physics B - Proceedings Supplements, Volumes 205206, Pages 36 - 41

[23] Orlando, 2013, *QCD results from ATLAS*, arXiv:1304.6895 [hep-ex]

[24] Sjöstrand et al., 2006, *PYTHIA 6.4 physics and manual*, Journal of High Energy Physics, Volume 2006, Issue 5, Page 26

[25] Sterman, 2004, *QCD and Jets*, arXiv:hep-ph/0412013

[26] Thaler and Wang, 2008, *Strategies to Identify Boosted Tops*, Journal of High Energy Physics, Volume 2008, Issue 07, Page 92

[27] Whalley et al., 2005, *The Les Houches Accord PDFs (LHAPDF) and Lhaglue*, arXiv:hep-ph/0508110